Efficiency Roadmap for Evolutionary Upgrades of PERC Solar Cells by TOPCon: Impact of Parasitic Absorption

Christoph Messmer, Andreas Fell, Frank Feldmann, Nico Wöhrle, Jonas Schön, Martin Hermle

Abstract— **Passivating contacts created via a thin interfacial oxide and a highly doped polysilicon layer, e.g. the TOPCon technology, are on the verge of being implemented in solar cell mass production. Investment decisions rely on R&D to identify the most promising implementation option, meaning a trustworthy roadmap based on predicted performance gains. This work shows how to thoroughly quantify the performance potential via numerical simulation, focusing on an evolutionary upgrade of a busbarless p-type bifacial PERC technology. We specifically highlight the need to consider not only the electrical gains of passivating contacts, but also the associated optical losses due to parasitic absorption in the polysilicon layers for front and rear illumination. The influence of free-carrier absorption (FCA) in polysilicon on the solar cell optics is characterized on experimental test structures in order to verify our optical simulation model. Introducing TOPCon fully at the rear and also locally aligned to the front fingers can boost the PERC efficiency by approximately 1%$_{abs}$. The final device is strongly limited by losses in the p-type c-Si bulk and phosphorus-doped front emitter. Consequently, the presented evolutionary TOPCon upgrades may well be of increased relevance for future improved p-PERC cells, as an alternative to the current focus on n-type TOPCon cells with boron emitter.**

Index Terms— **Passivating Contacts, TOPCon, Roadmap, Simulation, Parasitic absorption, Free-carrier absorption, Sentaurus TCAD, Quokka3**

I. Introduction

Passivating contacts created via a thin interfacial oxide and a highly doped polysilicon layer, e.g. the TOPCon technology by Fraunhofer ISE [1], are currently being evaluated concerning their suitability for mass production. The high potential of TOPCon and similar technologies have been proven by laboratory solar cells reaching ~ 26% efficiency [2, 3]. Consequently, a focus of the current global silicon solar cell R&D is to establish mass production compatible processes to transfer the technology to industry. While sharing the common goal of minimizing contact recombination, there are several possibilities of how to integrate TOPCon via various cell architectures into industrial cells. One approach is to apply TOPCon in an evolutionary manner to the PERC technology by either replacing the full rear side with p-type TOPCon, and/or by replacing the local phosphorus emitter by n-TOPCon on the front side. This might require the fewest changes to the current standards of industrial PERC mass production by sticking to p-type material and a phosphorus diffused front emitter. A more fundamental change not investigated in this paper would be to replace the bulk material by n-type c-Si and using a boron-doped front emitter. In any way, educated decisions are required to direct investment into the most promising routes, i.e. creating a roadmap based on expected performance gains.

This work shows how to thoroughly quantify the performance potential via numerical device simulation. We specifically highlight the need to fully consider not only the electrical gains, but also the associated optical losses, with the goal of extending the methodology of previous roadmaps [4, 5]. In this work we analyse an evolutionary TOPCon upgrade of a high efficiency bifacial PERC solar cell on p-type Cz wafers with screen-printed metallization and a zero busbar concept, with properties realistically achievable in industrial manufacturing. We explicitly consider the parasitic absorption within the polysilicon layers which (partly) compensate the electrical gains of TOPCon. The influence of free-carrier absorption (FCA) in polysilicon on the solar cell optics is characterized on experimental test structures in order to verify our optical simulation model. To the best knowledge of the authors, this is presented for the first time in this detail and allows us to make a more trustworthy prediction of the efficiency potential, including both mono- and bifacial illumination.

Manuscript received August 24th, 2019; revised October 11th, 2019; accepted November 23rd, 2019

The authors are with the Fraunhofer Institute for Solar Energy Systems ISE, Heidenhofstr. 2, 79110 Freiburg, Germany (corresponding author e-mail: christoph.messmer@ise.fraunhofer.de). J. Schön and C. Messmer are also with the Laboratory for Photovoltaic Energy Conversion, Department of Sustainable Systems Engineering (INATECH), University of Freiburg, Emmy-Noether-Str. 2, 79110 Freiburg, Germany.

II. Simulation Method

Optical modelling of the cell architectures is performed with Sentaurus TCAD [6] using raytracing combined with the Transfer-Matrix-Method (TMM). All thin-layers at the front and the rear side are modelled via TMM, which takes into account the refraction and parasitic band-to-band and free-carrier absorption (FCA) of the incoming light. Our simulation model effectively describes the roughness of the rear side by a combination of a rear angle and the Phong diffusion model [7, 8]. The free-carrier absorption in the poly-Si regions was described as suggested in [9] by the parametrization for crystalline Si by Baker-Finch [10]:

$$\alpha_{\mathrm{FCA}}^{\text{poly-Si}} = C \cdot N_{\mathrm{D}} \cdot \lambda^{\gamma}$$

where α is the FCA coefficient; C and γ are parametrization parameters, λ is the wavelength and N_D the doping

DOI: 10.1109/JPHOTOV.2019.2957642

concentration of the poly-Si layer. The optical model allows for bifacial illumination (details are listed in Table I).
Subsequently, 3D electrical modelling of the cell architectures is performed using Quokka3 [11, 12] with a 'zero busbar' symmetry element. This means that finger resistance as well as busbar shading and recombination is neglected in the simulation, essentially assuming a busbar-less interconnection concept. For both PERC and TOPCon a low contact resistivity was previously measured [13–16]. Since these values result in a relatively small cell performance loss, and because there is no clear quantitative difference between PERC and TOPCon contact resistivity, we assume the same low (ohmic) value of 1 mΩ/cm² for front and rear contacts in both concepts (PERC and TOPCon). We however stress the importance of achieving such low values with TOPCon technology, and advise to include the effect of contact resistivity in future works based on a thorough characterization.

Figure 1 on the left shows a bifacial PERC cell which is used as a reference and starting point with 23.25% front efficiency representing a high-end industrial solar cell with zero busbar design, which we will refer to as 'cell A'. For all cell structure variations the front and rear finger pitch was optimized in order to reach the highest efficiency.

Our choice of parameters for the electrical simulation, listed in Table II, is our best guess in accordance with literature ([4, 5, 8, 15, 17]). Many of those parameters may be substantially different to actual cells from different manufacturers; however the main point is not the choice of parameters, but to showcase the methodology, which in particular thoroughly considers the trade-off between electrical gains and optical losses when introducing TOPCon. Proceeding from this PERC cell reference (Figure 1, left) we investigate two TOPCon upgrades as shown in Figure 1 on the right (see also list of varied parameters in Table II):

I. **Full Rear** is featuring a full-area rear p-type TOPCon with a poly-Si thickness of 60 or 140 nm (R_S = 320 or 137Ω/□, $j_{0,pass,p\text{-}TOPCon}$ = 5 fA/cm² [14, 17]) and with a rear dielectric and local contacts with slightly higher recombination ($j_{0,met}$ = 20 fA/cm²). Since TOPCon allows for screen-printing of Ag-fingers instead of Al, we take the same finger width of 45 µm as on the front side. The optical properties of TOPCon were verified by reflection transmission measurements of experimental test structures as addressed in the next section. The charge carrier mobility in the poly-Si layer is taken from [9].
II. **Local Front** features an n-type TOPCon with a poly-Si thickness of 60 or 140 nm aligned to the front contact (w_{TOPCon} = 135 µm, $w_{Contact}$ = 45 µm). Due to screen-printing of the metal we assume the recombination underneath the contact to be $j_{0,met,n\text{-}TOPCon}$ = 20 fA/cm². The optical properties of n-TOPCon are modelled analogously to step I, fully considering parasitic absorption through band-band and free-carrier absorption.
III. **Fully TOPCon-upgraded p-PERC** combines steps I) Full Rear and II) Local Front. We will refer to this as the 'final' cell B.

III. Verification of Optical Model

To the best knowledge of the authors, a predictive optical cell model including the parasitic absorption in the poly-Si layers of TOPCon has not been published yet. Therefore, we will first validate the optical model of our simulations in this chapter using reflection and transmission measurements on experimental test structures.

We prepared two experimental structures optically similar to final non-metallized solar cells, with and without TOPCon on the rear side. The reference structure features a textured ARC coated front side and a saw-damage-etched, ARC-coated rear side. The reflection and transmission for front and rear illumination were measured by a spectrometer and are shown in Figure 2a and c as blue and red dotted lines, respectively. The experimental absorption was calculated by 1 – R – T and is shown as green dotted line. Moreover, both Figure 2a and c show the simulated RTA for front and rear illumination as solid lines. One can see that the overall agreement of simulated and measured data is good. However, Figure 2a shows that our simulation slightly overestimates the measured reflection and transmission by 5%$_{abs}$ for wavelengths greater than 1200nm. Therefore, the FCA of the c-Si bulk (highlighted by the arrows) is slightly lower than the measured absorption. For rear illumination shown in Figure 2c we see that for λ > 1200 nm both the reflection and transmission match the measured data and also the FCA in the c-Si bulk (see arrow).

Our second experimental cell structure includes a 150 nm n-type TOPCon layer on the rear side for which the measured

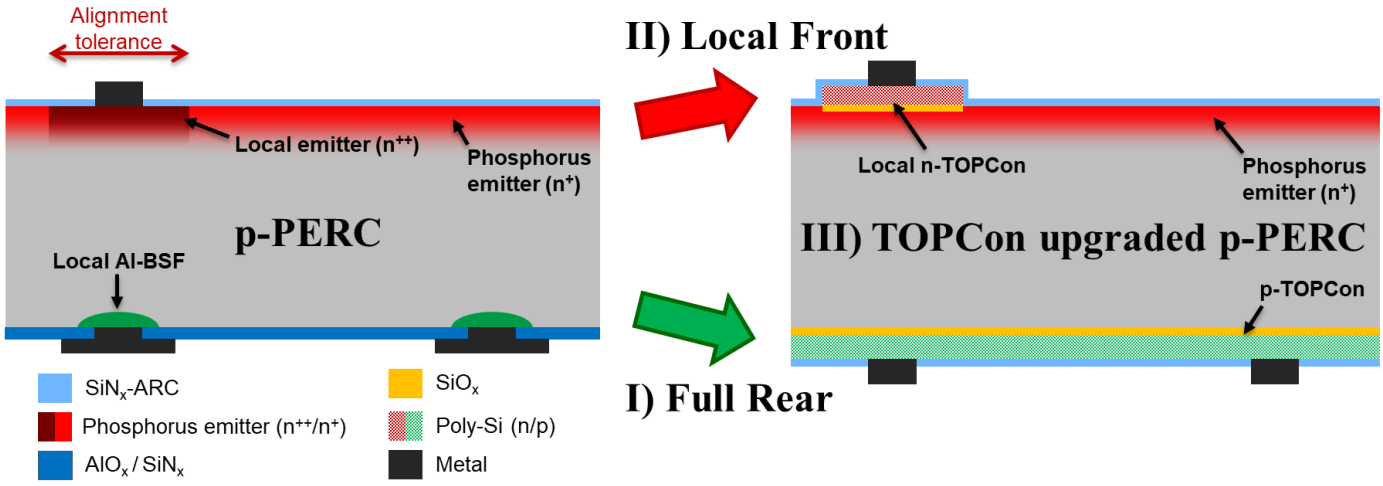

Figure 1: *Investigated cell architectures. On the left: A standard industrial PERC cell as reference. On the right: Two TOPCon upgrade architectures: I) Full Rear: Full-area rear p-type TOPCon with rear dielectric and local contact openings. II) Local Front: n-type TOPCon locally aligned to front contacts. III) Combination of I and II. Note that the texturing of the front surface is not depicted.*

DOI: 10.1109/JPHOTOV.2019.2957642

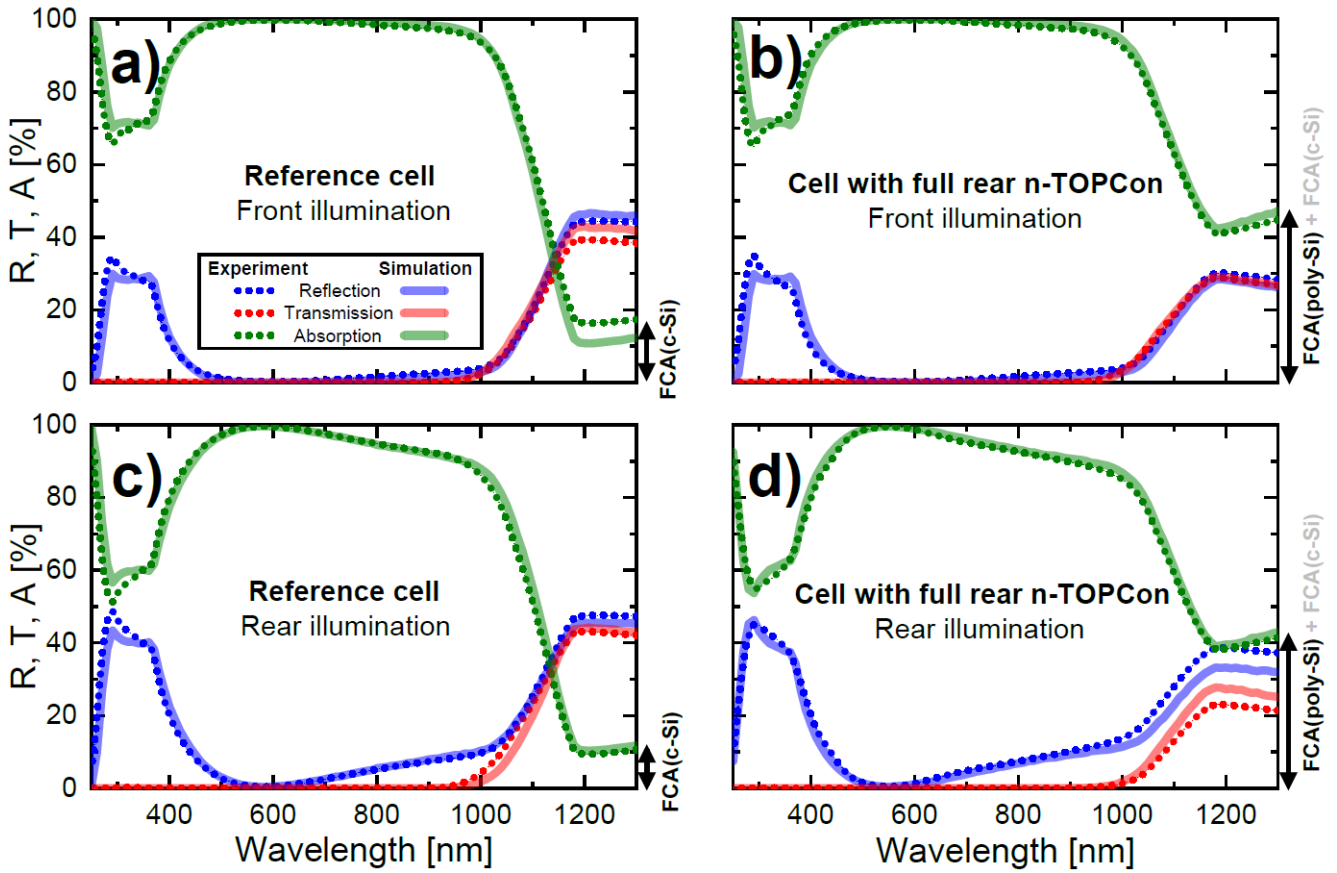

Figure 2: *Reflection, transmission and absorption data shown in red, blue and green, respectively. A reference cell without poly-Si is shown in (a) and (c) for front and rear illumination. The data for a cell with a 150 nm thick n-TOPCon on the rear side is shown in (b) and (d) for front and rear illumination. The experimental data is shown as dotted curves; the simulated data is shown as solid lines. The free-carrier absorption (FCA) is indicated by arrows.*

and simulated RTA data is shown for front and rear illumination in Figure 2b and Figure 2d, respectively. We can see that the simulation model predicts the increased absorption due to FCA above 1200 nm very well for a poly-Si doping of $N_D = 1.3 \cdot 10^{20}$ cm^{-3}, which is consistent with the measured sheet resistance and recent mobility measurements [18]. Figure 2d shows some deviations of the reflection and transmission above 1000 nm, possibly due to the rough rear surface which we only effectively describe by Phong diffusion and a rear angle in the simulation. However, the 5% lower reflection and 5% higher transmission cancel out to still match the absorption (as shown by the arrow in Figure 2d).

As a result, we see that our simulation approach combined with the Baker-Finch parametrization is useful to describe the effect of FCA in the n-type TOPCon layers, which means they can optically be well described as doped crystalline silicon. In the following we also use the Baker-Finch parametrization for the FCA in p-type TOPCon.

IV. Efficiency Potential of TOPCon on PERC

A. *Influence of Electrical Gains and Optical Losses on the Maximum Power Output*

By means of the simulation model and the choice of parameters (Table I and Table II) we now showcase the roadmap highlighting the role of the optical losses. Figure 3a shows the power output at maximum power point p_{mpp} for the cell architectures presented in Figure 1 with one sun front illumination (in this case equal to the cell efficiency in %). Starting from the 23.25%-PERC reference (cell A) the front and rear TOPCon upgrades are applied. For each step the electrical gains and optical losses are shown separately:

I. Full Rear (green): The simulations show that ~0.4%$_{abs}$ efficiency is possible to gain electrically with reduced rear recombination. In terms of electrical gains, thicker TOPCon layers are slightly more beneficial due to higher lateral conductance towards the metal contacts (as shown for the green dotted curve with 140 nm p-type TOPCon). However, when additionally considering the optical losses, we see that thicker TOPCon layers (dotted green) are in total less beneficial than thin layers (solid green), mostly due to free-carrier absorption (FCA) in the poly-Si(p) layer. In terms of efficiency this results in a loss of 0.1-0.2%$_{abs}$.

II. Local Front (red): For the locally aligned n-type TOPCon on the front side we see the same trend as for step I, but with a slightly lower absolute gain in efficiency, ~0.3%$_{abs}$. However, depending on the n-TOPCon thickness (60 nm solid, 140 nm dotted) more than half of the electrical gains are compensated by optical losses, even though TOPCon is only locally applied. The optical losses on the front side are dominated by parasitic absorption of light with short wavelengths, whereas FCA plays a secondary role. The optical losses have to be countered by reducing the width of the local TOPCon region beneath the metal finger which requires an improved alignment in the printing process (the influence of alignment will be shown in the following step)

DOI: 10.1109/JPHOTOV.2019.2957642

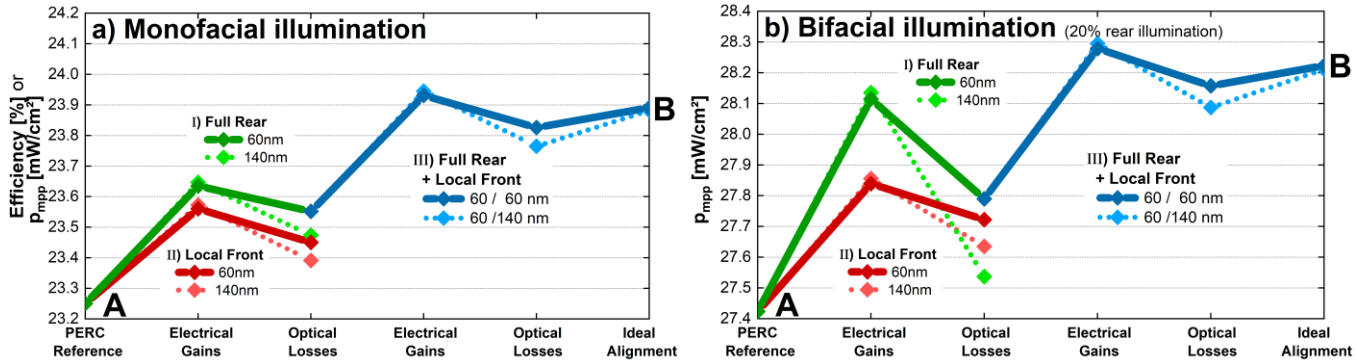

Figure 3: *Two roadmaps showing the power at maximum-power-point (MPP) for a zero busbar design starting from a PERC reference cell (cell A) under (a) only front illumination of one sun or (b) additional 20% rear illumination (bifacial illumination). In a first step the TOPCon upgrades are applied as introduced in Figure 1, first by only replacing either the rear side (I, green) or the front side (II, red). The electrical gains and optical losses (including free-carrier absorption, FCA) are separately shown for two different poly silicon layer thicknesses (solid for 60nm, dotted for 140nm). Step III in blue shows the combination of both I and II and the influence of ideal alignment of the metal fingers on the local n-TOPCon at the front (cell B).*

III. Full Rear + Local Front (blue): Proceeding from step I for a 60nm p-TOPCon full rear side, we additionally apply the local TOPCon (step II) in order to get the final structure. For our set of cell parameters, the electrical gains again reach ~0.4%$_{abs}$, which is higher than step II alone, due to synergy effects. However, another 0.1-0.2%$_{abs}$ in efficiency is lost due to parasitic absorption in the local front n-TOPCon layer. In a last step the influence of contact alignment is investigated. Since optical losses are critical in the local front TOPCon region, it is beneficial to reduce the TOPCon width to the contacts width (in this work from 135 µm to 45 µm). Technologically this comes at the cost of a higher requirement on precise contact alignment. Figure 3a shows that an improvement of around 0.1%$_{abs}$ can be achieved by aligning the local n-TOPCon ideally to the region underneath the contact ($w_{TOPCon} = w_{Contact}$ = 45 µm, denoted as 'cell B').

Once again, we emphasize, that the absolute numbers of these electrical gains and optical losses depend on the initial reference cell and parameter assumptions (e.g. $j_{0,met}$). However, this roadmap showcases the importance of thoroughly taking into account both electrical gains and optical losses.

Since bifacial applications of solar cells become even more important in the future, we show the same roadmap with additional rear illumination of 20% AM1.5g spectrum in Figure 3b. One can see that this roadmap starts with a maximum power output density p_{mpp} of 27.4 mW/cm² for the PERC reference. When applying the TOPCon upgrades we see the following for a bifacial application (Figure 3b):

I. Full Rear (green): The electrical gain of 0.7 mW/cm² is higher than for front illumination only, however, depending on the p-TOPCon thickness, around 0.3-0.6 mW/cm² are compensated by optical losses. These optical losses are relatively high due to additional parasitic absorption of light from the rear side in the full-area TOPCon layer for short wavelengths (in addition to FCA).

II. Local Front (red): The electrical gain is higher than for only front illumination, whereas the optical loss is in the same range.

III. Full Rear + Local Front (blue): Under bifacial illumination cell B gains 0.8 mW/cm² in total compared to cell A.

One can see, that it depends on the illumination setup and the choice of cell parameters, whether Full Rear or Local Front is a better option for a first evolutionary step towards a TOPCon based industrial cell. However, in any case, Figure 3 highlights that optical losses are substantial and should be quantitatively taken into account when we want to make a reasonable choice on the next evolutionary steps of the PERC cell technology towards passivating contacts like TOPCon.

B. Electrical loss analysis

Figure 4A shows the free energy loss analysis (FELA, [19]) for the PERC reference under bifacial illumination (cell A in Figure 3b). The electrical losses on the left show that the bulk (grey) and the phosphorus front emitter (light red) both account for around a third of the total electrical losses. The remaining third of the losses is made up by the regions that are going to be optimized by the two TOPCon upgrades, namely the local front emitter (red and dark red) and rear side (green and dark green). The contribution of the front and rear contact resistivity is included in the share of front and rear contact.

Figure 4B shows the electrical loss analysis for the final upgraded cell architecture (cell B in Figure 3b). The total electrical losses were lowered by about 25% compared to PERC, and the two TOPCon upgrades on the front and rear minimized the corresponding electrical losses to a share of about 15% (see brace in Figure 4B). However, this gain is partly compensated by the phosphorus diffused front emitter (shown in light red) whose electrical losses absolutely increase by 0.16 mW/cm² (this is 25% of the electrical gains) due to synergy effects. Electrically, cell B is now almost completely

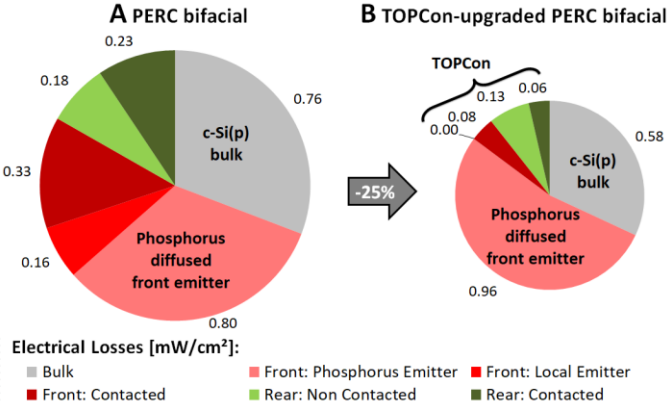

Figure 4: *Electrical loss analysis (FELA) for both PERC (cell A) and the final TOPCon-upgraded cell (cell B) under bifacial illumination.*

DOI: 10.1109/JPHOTOV.2019.2957642

limited by the phosphorus diffused front emitter (53%, with R_{sheet}=149 Ω/□ and j_0=30 fA/cm², see Table II in the appendix) and the p-type silicon bulk (32%), being also the main reason for the only moderate absolute efficiency improvement to still below 24%. This explains why a more substantial efficiency improvement is only possible by improvement of the phosphorus emitter or a change to n-type silicon bulk material (with a boron emitter and full-area rear n-TOPCon), the latter being the current focus of industrialization. This will be further discussed in chapter V.

C. Optical loss analysis

Figure 5 shows the optical losses taken from current loss analysis as a bar chart for the PERC ('cell A', patterned bars) and TOPCon cell ('cell B', blank bars). The first pair of bars shows the shading losses of the metal fingers (shown as grey bars). This optical loss is similarly high for both cell concepts (~1.7 mA/cm²), since two opposing effects compensate each other: On the one hand, TOPCon has an optical benefit in rear shading due to its smaller rear finger width (45µm Ag-fingers instead of 100µm Al-fingers for PERC). On the other hand, shading increases for TOPCon due to smaller optimum finger pitch on the front side (see also to Table II).

The second pair of bars shows the incoupling losses due to external reflection and parasitic band-to-band absorption which occur when the front (rear) illumination is impinging for the first time on the front (rear) layers. The external reflection R_{ext} is equally high for both cell concepts (~1.56 mA/cm², shown in light blue). The parasitic absorption in the anti-reflection coating (ARC) is shown in yellow which is equally high for both PERC and TOPCon. However, the TOPCon layers add to the parasitic band-to-band absorption with 0.09 mA/cm² in the local front poly-Si(n) (shown in orange) and another 0.41 mA/cm² for the full rear poly-Si(p) (shown in dark blue), whereby the latter losses only occur for bifacial illumination.

The third pair of bars in Figure 5 shows the imperfect light-trapping and FCA of the photons once they are bouncing inside the wafer. This includes escape reflection R_{esc} and transmission T in the range of long wavelengths (~2.4 mA/cm² for PERC, and ~2.1 mA/cm² for TOPCon, shown as red bars). Parasitic absorption due to free-carrier absorption (FCA) is shown in green for the crystalline silicon bulk (~0.43 mA/cm² for PERC, and ~0.39 mA/cm² for TOPCon) and in dark blue for the full rear p-TOPCon layer (~0.44 mA/cm²). Despite these high FCA losses in TOPCon, the overall losses according to imperfect light trapping is only rising by 0.16 mA/cm² with respect to PERC, since the share of R_{esc}, T and FCA in the c-Si bulk is getting smaller due to synergy effects. Further note, that most of the imperfect light trapping losses are inevitable. Employing the limit defined by Green [20] gives a figure of merit for the inevitable losses, which is approx. 2 mA/cm² for both PERC and TOPCon-upgraded cell.

To sum up, one can see that the optical properties of PERC are better and it is very important to take the optical losses of TOPCon into account for an appropriate description of efficiency potentials.

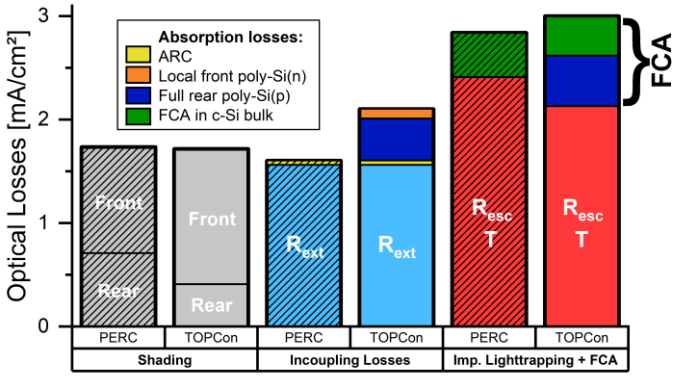

Figure 5: *Optical loss analysis for both PERC ('cell A') and TOPCon on both sides ('cell B') under bifacial illumination (20% rear illumination), resolved in shading of front and rear metal fingers (grey), incoupling losses and imperfect light trapping and FCA. More details see paragraph IV.C*

D. Influence of the illumination spectrum

Besides the rear illumination intensity (which is assumed to be 20% of AM1.5g to this point), also the spectral distribution of the illumination intensity is influential when the optical properties of the PERC technology are compared to TOPCon.

Figure 6 shows the simulated external quantum efficiency (EQE) for both PERC ('cell A') and TOPCon-upgraded cell ('cell B'). The EQEs of PERC and TOPCon for the front side (shown in black and red, respectively) are almost identical, apart from the slightly lower EQE for TOPCon above 1000 nm due to FCA in the poly-Si layers. However, the EQEs for rear illumination of PERC and TOPCon (shown in blue and green) are quite distinct. We see that the TOPCon cell is disadvantageous for rear illumination with wavelengths smaller than 500nm due to parasitic absorption in the TOPCon layers. However, for wavelengths greater than 600nm, the EQE of the TOPCon-upgraded cell is better than for PERC, due to better electrical properties and smaller finger pitches. As a consequence red-shifted spectral distributions are beneficial for bifacial TOPCon relative to PERC devices, such as it is the case for the albedo of many different grounds like brick or grass [21, 22].

Figure 7 shows the bifaciality of PERC ('cell A', patterned bars) and TOPCon-upgraded cell ('cell B', blank bars) for different rear illumination spectra. The light blue pair of bars to the left show the bifaciality factor $\beta_{\uparrow\downarrow}$ according to the standard definition of bifaciality:

$$\beta_{\uparrow\downarrow,\text{standard}} = \frac{\eta_{\uparrow}(\text{AM1.5g})}{\eta_{\downarrow}(\text{AM1.5g})}$$

where $\eta_{\downarrow}$ ($\eta_{\uparrow}$) is the efficiency for front (rear) illumination with 1 sun of AM1.5g. We see that the PERC and TOPCon-upgraded cell show a very similar bifaciality ($\beta_{\uparrow\downarrow}$~90%). We note that the uncommonly high PERC bifaciality is due to overall high quality of assumed cell parameters, as well as the

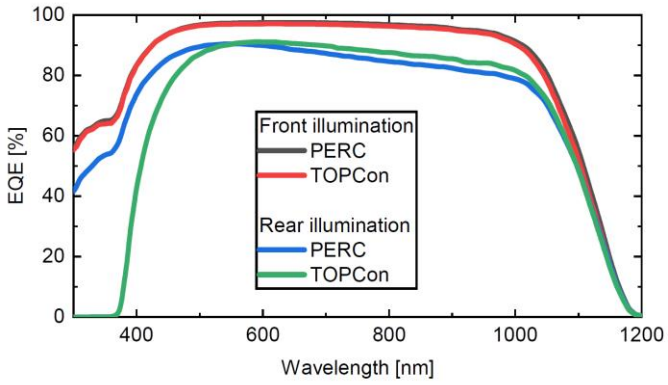

Figure 6: *Simulated external quantum efficiency (EQE) for PERC (cell A) and TOPCon on both sides (cell B) for front illumination (black and red, respectively) and rear illumination (blue and green, respectively).*

DOI: 10.1109/JPHOTOV.2019.2957642

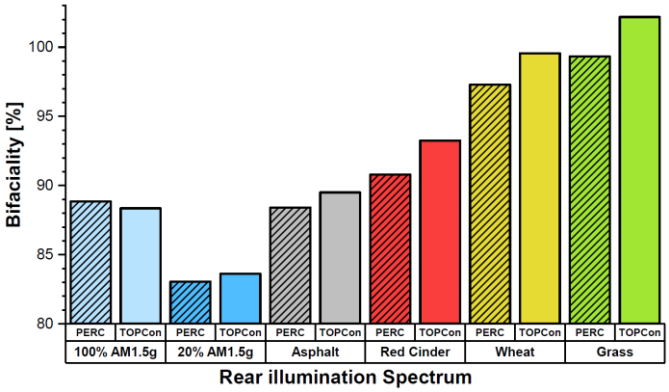

Figure 7: *Bifaciality factor of PERC (patterned bars) and the TOPCon-upgraded cell (black bars) for different rear illumination spectra. The first group is according to the standard definition of the bifaciality using 1 sun of AM1.5g. The other spectra were adopted from [22].*

assumed zero-busbar concept, which in particular results in rear metallization fractions lower than the current industrial standard. Our simulations thereby also suggest that bifacial PERC cells approaching 90% bifaciality is realistic. To compare different rear illumination spectra, we extended the standard definition of the bifaciality to arbitrary rear illumination spectra:

$$\beta_{\uparrow\downarrow} = \frac{\eta_{\uparrow}(\text{rear spectrum})}{\eta_{\downarrow}(\text{AM1.5g})}$$

where we used measured albedos of different grounds (AM1.5g scaled by reflectivities extracted from [22]) in order to calculate $\eta_{\uparrow}$(rear spectrum), and integrate front and rear spectrum to 1200nm to calculate the incident intensity. Figure 7 shows the bifaciality of both PERC and the TOPCon-upgraded cell for a rear illumination spectrum of 20% AM1.5g in dark blue. One can see that the bifaciality drops to $\beta_{\uparrow\downarrow}$~83%, with the drop being somewhat less for TOPCon.

When more realistic albedos are assumed (like asphalt, red cinder, wheat, grass shown in grey, red, yellow and green, respectively) we see that the bifaciality factor increases for both PERC and TOPCon, since the red-shifted spectra are better for both cell concepts. However, we see that the difference in bifaciality factor between PERC and TOPCon gets bigger to the benefit of the TOPCon concept. This gives an additional advantage of TOPCon over PERC in a bifacial deployment commonly not considered in roadmaps, which in particular holds for agro-photovoltaics with grass-like albedo.

V. Outlook: Influence of Future PERC Improvements

The last chapter has shown that front and rear TOPCon upgrades on the current mainstream p-PERC technology achieve efficiency gains of below 1%$_{abs}$ (Figure 3). The final TOPCon-upgraded p-PERC cell is highly limited by specific PERC features like the p-type c-Si bulk and the phosphorus-doped front emitter (Figure 4). However, as we will discuss in the following, evolutionary TOPCon upgrades benefit from ongoing development of the p-PERC technology in the future.

Figure 8 to the left shows the power output density for the PERC and TOPCon-upgraded cell as black and blue data point, respectively, with the parameters as used throughout this paper ('reference') leading to a gain in power output of 0.7 mW/cm² (green arrow, corresponding to Figure 3b).

Subsequently, we assume an exemplary 'future' scenario, including smaller finger widths, an improved phosphorus-

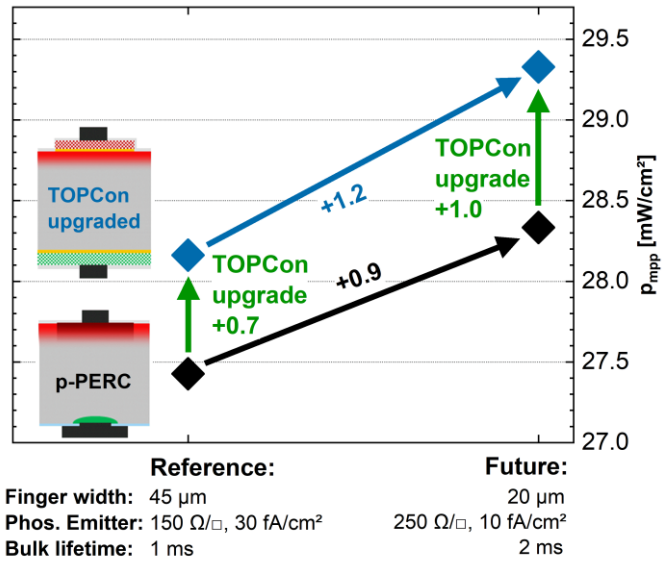

Figure 8: *Simulated power output density (p_{mpp}, 20% illumination from the rear side) for both PERC and TOPCon-upgraded cell, shown in black and blue, respectively. The reference scenario (on the left) shows the p_{mpp} for the parameters used in this paper, the 'future' scenario (on the right) shows a possible development of the PERC technology, leading to an improvement of PERC (black arrow) and likewise to an even more improved TOPCon upgraded future cell (blue arrow).*

doped emitter and higher bulk lifetime (see parameters to the right in Figure 8, 'future'). Note, that these improvements are not based on current experiments, but sketch a possible future scenario based on predictions extrapolated from the past development [23]. The black arrow shows the predicted power gain of the PERC cell (0.9 mW/cm²) for this exemplary future development. However, the TOPCon-upgraded cell also benefits from these PERC developments, leading to an even higher gain of the p_{mpp} (1.2 mW/cm², blue arrow). The difference in power output between the PERC cell and the TOPCon-upgraded cell even increases with 0.7 mW/cm² for 'reference' scenario to 1.0 mW/cm² for the 'future' scenario (as shown by the grey arrows) due to synergy effects.

VI. Conclusion

In this paper we highlighted the importance to fully take into account the optical effects of current solar cell technologies in order to obtain reliable efficiency predictions from simulation. We presented a simulation model which is able to describe the optics of PERC and TOPCon solar cells, especially accounting for the parasitic absorption in the doped poly-Si layers including free-carrier absorption (FCA).

We verified our simulation model against reflection and transmission measurements allowing predictive simulations of efficiency potentials. We showcased an evolutionary roadmap from p-PERC by including TOPCon technologies on the front and/or rear side, where both electrical gains and optical losses were differentiated. It showed that TOPCon upgrades yield electrical gains due to reduced contact recombination, which however are substantially lowered by the introduced parasitic absorption in the poly-Si layers resulting in an overall gain of somewhat below 1%$_{abs}$. Our loss analysis on the final TOPCon-upgraded p-PERC cell reveals that its efficiency is strongly limited by PERC features like the phosphorus diffused front emitter and p-type bulk to below 24%. This

DOI: 10.1109/JPHOTOV.2019.2957642

explains why evolutionary TOPCon upgrades on current p-type PERC solar cells are limited in potential performance gains, which motivates a switch to n-type bulk material and boron-doped emitter, as currently pursued by industry. However, we have shown that the presented integration of TOPCon on p-PERC as an evolutionary upgrade may well be an attractive option, since the TOPCon-upgraded cell benefits from the ongoing mainstream development of the p-PERC technology.

ACKNOWLEDGMENT

This work was supported by the German Federal Ministry for Economic Affairs and Energy BMWi and by industry partners within the research project "GENESIS" under contract No. 0324274C and 0324274E. The authors are responsible for the content. C. Messmer gratefully acknowledges the scholarship of the German Federal Environmental Foundation ("Deutsche Bundesstiftung Umwelt").

VII. REFERENCES

[1] F. Feldmann, M. Bivour, C. Reichel, H. Steinkemper, M. Hermle, and S. W. Glunz, "Tunnel oxide passivated contacts as an alternative to partial rear contacts," *Sol. Energy Mater. Sol. Cells*, vol. 131, pp. 46–50, 2014.

[2] A. Richter, J. Benick, F. Feldmann, A. Fell, M. Hermle, and S. W. Glunz, "n-Type Si solar cells with passivating electron contact: Identifying sources for efficiency limitations by wafer thickness and resistivity variation," *Sol. Energy Mater. Sol. Cells*, vol. 173, pp. 96–105, 2017.

[3] F. Haase, C. Hollemann, S. Schäfer, A. Merkle, M. Rienäcker, J. Krügener, R. Brendel, and R. Peibst, "Laser contact openings for local poly-Si-metal contacts enabling 26.1%-efficient POLO-IBC solar cells," *Sol. Energy Mater. Sol. Cells*, vol. 186, pp. 184–193, 2018.

[4] B. Min, M. Muller, H. Wagner, G. Fischer, R. Brendel, P. P. Altermatt, and H. Neuhaus, "A Roadmap Toward 24% Efficient PERC Solar Cells in Industrial Mass Production," *IEEE J. Photovoltaics*, vol. 7, no. 6, pp. 1541–1550, 2017.

[5] L. Tous *et al., Eds., Efficiency Roadmaps for Industrial Bifacial pPERC and nPERT Cells*. SiliconPV 2019, Leuven.

[6] Synopsis, "Sentaurus Device User Guide: release L-2016.03-SP2," http://www.synopsys.com, 2016.

[7] D. Kray, M. Hermle, and S. W. Glunz, "Theory and experiments on the back side reflectance of silicon wafer solar cells," *Prog. Photovolt: Res. Appl.*, vol. 16, no. 1, pp. 1–15, 2008.

[8] A. Fell, K. R. McIntosh, P. P. Altermatt, Janssen, G. J. M., R. Stangl, A. Ho-Baillie, H. Steinkemper, J. Greulich, M. Müller, B. Min, K. C. Fong, M. Hermle, I. G. Romijn, and M. D. Abbott, "Input parameters for the simulation of silicon solar cells in 2014," *IEEE Journal of Photovoltaics*, vol. 5, no. 4, pp. 1250–1263, 2015.

[9] F. Feldmann, M. Nicolai, R. Müller, C. Reichel, and M. Hermle, "Optical and electrical characterization of poly-Si/SiO x contacts and their implications on solar cell design," *Energy Procedia*, vol. 124, pp. 31–37, 2017.

[10] S. C. Baker-Finch, K. R. McIntosh, D. Yan, K. C. Fong, and T. C. Kho, "Near-infrared free carrier absorption in heavily doped silicon," *J. Appl. Phys.*, vol. 116, no. 6, p. 63106, 2014.

[11] A. Fell, J. Schön, M. C. Schubert, and S. W. Glunz, "The concept of skins for silicon solar cell modeling," *Sol. Energy Mater. Sol. Cells*, vol. 173, pp. 128–133, 2017.

[12] A. Fell, *quokka3*. [Online] Available: www.quokka3.com. Accessed on: Jan. 22 2018.

[13] S. Mack, J. Schube, T. Fellmeth, F. Feldmann, M. Lenes, and J.-M. Luchies, "Metallisation of Boron-Doped Polysilicon Layers by Screen Printed Silver Pastes," *Phys. Status Solidi RRL*, vol. 214, p. 1700334, 2017.

[14] P. Padhamnath, J. Wong, B. Nagarajan, J. K. Buatis, L. M. Ortega, N. Nandakumar, A. Khanna, V. Shanmugam, and S. Duttagupta, "Metal contact recombination in monoPoly™ solar cells with screen-printed & fire-through contacts," *Solar Energy Materials and Solar Cells*, vol. 192, pp. 109–116, 2019.

[15] A. Fell and P. P. Altermatt, "A Detailed Full-Cell Model of a 2018 Commercial PERC Solar Cell in Quokka3," *IEEE Journal of Photovoltaics*, vol. 8, no. 6, pp. 1443–1448, 2018.

[16] F. Feldmann, T. Fellmeth, B. Steinhauser, H. Nagel, D. Ourinson, S. Mack, E. Lohmüller, J. Polzin, J. Benick, A. Richter, A. Moldovan, M. Bivour, F. Clement, J. Rentsch, M. Hermle, and S. W. Glunz, "Large Area TOPcon Cells Realized by a PECVD Tube Process,"

[17] U. Römer, R. Peibst, T. Ohrdes, B. Lim, J. Krugener, T. Wietler, and R. Brendel, "Ion Implantation for Poly-Si Passivated Back-Junction Back-Contacted Solar Cells," (English), *IEEE J. Photovoltaics*, vol. 5, no. 2, pp. 507–514, 2015.

[18] M. Nicolai, M. Zanuccoli, F. Feldmann, M. Hermle, and C. Fiegna, "Analysis of Silicon Solar Cells With Poly-Si/SiO_x Carrier-Selective Base and Emitter Contacts," *IEEE J. Photovoltaics*, pp. 1–7, http://ieeexplore.ieee.org/ielx7/5503869/5986669/08168398.pdf?tp=&arnumber=8168398&isnumber=5986669, 2017.

[19] R. Brendel, S. Dreissigacker, N.-P. Harder, and P. P. Altermatt, "Theory of analyzing free energy losses in solar cells," *Appl. Phys. Lett.*, vol. 93, no. 17, p. 173503, 2008.

[20] M. A. Green, "Lambertian light trapping in textured solar cells and light-emitting diodes: Analytical solutions," *Prog. Photovolt: Res. Appl.*, vol. 10, no. 4, pp. 235–241, 2002.

DOI: 10.1109/JPHOTOV.2019.2957642

[21] M. R. Vogt, T. Gewohn, K. Bothe, C. Schinke, and R. Brendel, "Impact of Using Spectrally Resolved Ground Albedo Data for Performance Simulations of Bifacial Modules," (eng), 2018.

[22] D. E. Bowker, R. E. Davis, D. L. Myrick, K. Stacy, and W. T. Jones, "Spectral reflectances of natural targets for use in remote sensing studies," 1985.

[23] ITRPV consortium, "International Technology Roadmap for Photovoltaic: Results 2017 including maturity report 2018," 2018.

[24] *PV Lighthouse: SunSolve.* [Online] Available: www.pvlighehouse.com.au.

[25] C. Schinke, P. C. Peest, J. Schmidt, R. Brendel, K. Bothe, M. R. Vogt, I. Kröger, S. Winter, A. Schirmacher, S. Lim, H. T. Nguyen, and D. Macdonald, "Uncertainty analysis for the coefficient of band-to-band absorption of crystalline silicon," *AIP Advances*, vol. 5, no. 6, p. 67168, 2015.

[26] Malte Ruben Vogt, *Development of Physical Models for the Simulation of Optical Properties of Solar Cell Modules: PhD thesis*. Hannover, 2015.

[27] P. Kumar, M. K. Wiedmann, C. H. Winter, and I. Avrutsky, "Optical properties of Al 2 O 3 thin films grown by atomic layer deposition," *Applied optics*, vol. 48, no. 28, pp. 5407–5412, 2009.

TABLE I: OPTICAL SIMULATION PARAMETERS

Quantity	*Value*
Sentaurus TCAD	
Version	L-2016.03-SP2 [6]
Global	
Temperature	300 K
Spectrum	AM1.5g, 1 sun (from [24])
Crystalline Silicon	
Thickness	150 µm
Resistivity	1 Ωcm (n-type for RTA, p-type for roadmap)
Complex refraction data	Schinke et al. [25] extended with FCA model of Baker-Finch [10]
PERC	
Front layers	textured 75 nm SiN_x, Vogt et al. [26] 6 nm AlO_x, Kumar et al. [27]
Rear layer	etched, 75 nm SiN_x [26]
Full Rear TOPCon	
Anti-reflection coating	75 nm SiN_x, Vogt et al. [26]
Thickness Oxide	1.4 nm
Poly silicon complex ref. data	Schinke et al. [25] extended with FCA model of Baker-Finch [10]
Poly silicon thickness	150 nm for RTA (as experiment) 60/140 nm for roadmap
Poly silicon doping	$1.3 \cdot 10^{20}$ cm^{-3} (n-type for RTA, p-type for roadmap)
Local Front TOPCon	
same as full rear, but n-type	

TABLE II: ELECTRICAL SIMULATION PARAMETERS

Quantity	*Value*
Quokka3	
Version	1.2.6
Finger Pitches (optimized)	
PERC bifacial (Front | Rear)	1400 µm | 900 µm
TOPCon bifacial (Front | Rear)	1100 µm | 700 µm
Crystalline Silicon Bulk	
Resistivity	1 Ωcm, p-type
Recombination	Auger, SRH (τ_{min}=1 ms)
PERC	
Front finger width	45 µm (Ag)
Rear finger width	100 µm (Al)
Finger shading fraction	70%
Front contact width	45 µm
Rear contact width	60 µm (dashed contacts)
Contact resistivity	1 mΩ cm² (Front and rear)
Busbar	zero busbar concept
Phosphorus diffused front emitter	R_{sheet} = 148.8 Ω/□ [15] j_0 = 30.7fA/cm² [15]
Local front emitter	R_{sheet} = 58.5 Ω/□ [15] Collection efficiency = 88.2% [15] j_0 = 120 fA/cm² (non-contacted, [15]) $j_{0,met}$ = 800 fA/cm² (contacted, [5])
Full rear BSF	j_0 = 10 fA/cm² (non-contacted) $j_{0,met}$ = 400 fA/cm² (contacted, [4, 15])
Full Rear p-TOPCon	
same as for PERC except for:	
Rear finger width	45 µm (Ag, screen printing)
Rear contact width	45 µm (line contacts)
TOPCon sheet resistance	calculated from hole mobility μ_h=25 cm²/(Vs)
Recombination	j_0 = 5 fA/cm² (non-contacted) $j_{0,met}$ = 20 fA/cm² (contacted)
Local Front n-TOPCon	
same as for PERC, except for:	
Sheet resistance	calculated as parallel sheet resistance of TOPCon and phosphorus emitter
Recombination	j_0 = 20 fA/cm² (non-contacted) $j_{0,met}$ = 20 fA/cm² (contacted)

DOI: 10.1109/JPHOTOV.2019.2957642